Lagrangian Vortex computations of turbine wakes: recent improvements using Poletto's Synthetic Eddy Method (SEM) to account for ambient turbulence

Lagrangian Vortex computations of turbine wakes: recent improvements using Poletto's Synthetic Eddy Method (SEM) to account for ambient turbulence

Camille Choma Bex[⋆,†], Grégory Pinon[⋆], Myriam Slama[⋆], Benoist Gaston[#], Grégory Germain[†], Elie Rivoalen[⋆,¶]

[⋆] LOMC, Laboratoire Ondes et Milieux Complexes, Normandie Univ, UNIHAVRE, CNRS, LOMC, 76600 Le Havre, France
[†] IFREMER, Marine Structures Laboratory, 150 quai Gambetta, 62200 Boulogne-sur-mer, France
[#] CRIANN, Centre Régional Informatique et d'Applications Numériques de Normandie, 76800 Saint-étienne-du-Rouvray, France
[¶] LMN, Laboratoire de Mécanique de Normandie, Normandie Univ, INSA Rouen, LMN, 76000 Rouen, France

E-mail: gregory.pinon@univ-lehavre.fr

Abstract. This paper presents possible techniques for modelling ambient turbulence in the Lagrangian Vortex Method formalism. Due to the fact that regular Synthetic Eddy Method (SEM) already presented in previous studies is not divergence free by definition; improvements were necessary to develop a similar SEM method with such a divergence free property. The recent improvements formulated by R. Poletto give the way to such a possibility. This new Divergence Free Synthetic Eddy Method (DFSEM) is presented here in comparison with the regular SEM. Obtained numerical velocity fields are compared in terms of convergence properties, Power Spectral Density and also Taylor macro-scale. Finally, turbine wakes are computed with both the recent Poletto's DFSEM and the regular Jarrin's SEM to highlight differences. At this stage of development, the DFSEM seems very promising even though some improvements are still necessary.

1. Introduction

The computation of turbine wakes remains a challenge to the scientific community. Lagrangian methods offer alternatives to the many Eulerian approaches most commonly used such as in Bernard *et al.* [1] among others. A comprehensive review of these possibilities is given in the work of Hansen *et al.* [8]. Among these possibilities, Vortex methods are already in use in the wind energy sector [18, 17, 5, 6]. Unfortunately, ambient turbulence cannot be taken into account in the Lagrangian Vortex Method when using its Vortex blob approximation [11]. It is however possible to account for ambient turbulence under a Particle-Mesh approximation [3, 6]. A different approach is chosen for the present study: the Synthetic Eddy Method (SEM) initially developed by Jarrin *et al.* [9] is adapted to be integrated into the Lagrangian Vortex Blob formulation. A first version of the method was presented in Pinon *et al.* [14] which is now completed and more deeply analysed in Choma Bex *et al.* [2]. Finally, an alternative version of the SEM more recently proposed by Poletto [16] will be presented and analysed.

2. Numerical methods: Jarrin's and Poletto's formulations

This paper aims to show the implementation of the Synthetic Eddy Method (SEM) in the context of Lagrangian Vortex Blob method simulations. The initial version of the SEM given by Jarrin *et al.* [9] using a distribution of velocity sources and sinks to mimic ambient turbulence is first presented, followed by the divergence free adaptation (DFSEM) of Poletto [16].

Both formulations rely on the Reynolds decomposition of the upstream velocity vector field $\mathbf{u}_\infty(\mathbf{x},t)$:

$$\mathbf{u}_\infty(\mathbf{x},t) = \overline{\mathbf{u}_\infty}(\mathbf{x}) + \mathbf{u}'(\mathbf{x},t), \tag{1}$$

where bold symbols represent vectors, $\bar{\cdot}$ stands for the averaged value of any function $\cdot$ and $\cdot'$ its fluctuating part, which is here assumed to have a null average. Jarrin *et al.* consider the

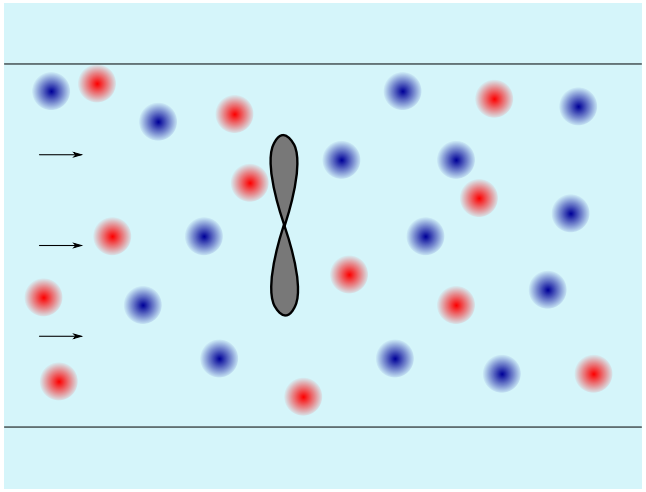

Figure 1. Definition of the *turbulent structures* (red and blue marks) immersed in the incoming flow. In the results presented in Section 3, no turbine is considered and in those of Section 4, the turbine blades will be taken into account.

fluctuating velocity u' as the velocity perturbation caused by N *turbulent structures* (see Fig. 1) randomly placed within a given study space of volume V_0:

$$\mathbf{u}' = \frac{1}{\sqrt{N}} \sum_{k=1}^{N} \mathbf{c^k} f_\lambda\left(\frac{\mathbf{x}-\mathbf{x}^k}{\lambda}\right). \tag{2}$$

In order to reproduce any desired turbulence intensity I_∞ and Reynolds stress tensor $\overline{\overline{R}}$, each *turbulent structure* is assigned an intensity $\mathbf{c_k}$ of its own:

$$c^k{}_i = \epsilon_i^k \sum_{j=1}^{3} a_{ij}, \tag{3}$$

where the Lund's coefficients a_{ij} [12] are based on the Cholesky decomposition of the Reynolds stress tensor $\overline{\overline{R}} = \overline{\overline{A}}\ {}^t\overline{\overline{A}}$:

$$a_{ij} = \begin{pmatrix} \sqrt{R_{11}} & 0 & 0 \\ R_{21}/a_{11} & \sqrt{R_{22}-a_{21}^2} & 0 \\ R_{31}/a_{11} & (R_{32}-a_{21}a_{31})/a_{22} & \sqrt{R_{33}-a_{31}^2-a_{32}^2} \end{pmatrix} = \overline{\overline{A}}. \tag{4}$$

The random nature of ambient turbulence is represented by the randomly assigned signs ϵ_i^k, which have an equal probability of being $+1$ or -1, as well as the initially random positioning of the *turbulent structures*. This sign will decide whether the structure is a velocity source ($\epsilon_i^k = +1$) or a velocity sink ($\epsilon_i^k = -1$) featured by the different colours depicted in Fig. 1.

As a reminder, the Turbulent Kinetic Energy (TKE) K is also calculated based on components of the Reynolds stress tensor:

$$K = \sqrt{R_{11} + R_{22} + R_{33}}, \tag{5}$$

and will be used in order to measure the accuracy of its reproduction.

To complete the definition of all the terms involved in equation (2), f_λ is the shape function that needs to respect some constraints in order to ensure statistical convergence of the imposed turbulence conditions, such as:

$$\begin{cases} f_\lambda \in \mathcal{C}^0(\mathcal{R}, \mathcal{R}) \\ f_\lambda(x) = 0 \ \forall \ x \ \notin [-\lambda, \lambda] \\ argmax(f_\lambda(x)) = 0 \\ f_\lambda(x) = f_\lambda(-x) \\ \int_{-\lambda}^{\lambda} f_\lambda^2(x)\,\mathrm{d}y = 1 \end{cases} \tag{6}$$

where λ is a length scale defining the area of influence of each turbulent structure.

A more detailed presentation of Jarrin's formulation can be found in [9, 10]. A recent adaptation of Jarrin's formulation to the Lagrangian Vortex Blob formalism is proposed in Choma Bex *et al.* [2], as well as alternative shape functions f_λ, convergence studies, and an evaluation of the generated turbulent length scales. As shown by the preliminary results presented in [2], the initial formulation of Jarrin *et al.* already gave interesting and promising results when integrated into the Lagrangian Vortex Blob formalism. However, one of the major drawbacks of Jarrin's SEM is that it is by definition not divergence-free, meaning that the incompressibility condition will not be verified in any such generated turbulent flows. This is caused by the fact that *turbulent structures* are formulated as velocity sources and sinks which prevent the velocity field from being divergence-free. Therefore, a new formulation of the *turbulent structures'* influence closer related to that of true vortices is necessary to overcome this constraint.

The more recent DFSEM (Divergence Free Synthetic Eddy Method) proposed by Poletto *et al.* [16] fulfills this requirement. This formulation has now been implemented in our numerical software showing promising results. This approach is based on a quasi-vortical formulation of the fluctuating velocity, which is closer to the Biot-Savart formulation used in the Vortex Method. Still based on the Reynolds decomposition of the velocity fields (eq. (1)), the new fluctuating velocity component $\mathbf{u'}$ is now defined as:

$$\mathbf{u'}(\mathbf{x}) = \frac{1}{\sqrt{N}} \sum_{k=1}^{N} \mathbf{K}_\lambda \left(\frac{\mathbf{x} - \mathbf{x^k}}{\lambda} \right) \times R(\mathbf{d^k}). \tag{7}$$

This last equation (7) has some similarities with its regular SEM counterpart (eq. (2)) in that it also relies on N *turbulent structures*, however here the vector $\mathbf{K}_\lambda$ is derived from the Biot-Savart Kernel such that $\mathbf{K}_\lambda(\mathbf{y}) = \frac{g_\lambda(|\mathbf{y}|)}{|\mathbf{y}|^3}$, with g_λ a suitable shape function. In this formulation, one such suitable function is defined as:

$$g_\lambda(y) = \begin{cases} \sqrt{\frac{V_0}{\pi\lambda^3}} (\sin(\pi y))^2 y \text{ for } |y| < 1, \\ 0 \text{ elsewhere.} \end{cases} \tag{8}$$

The result is given by the cross product of this modified kernel by turbulent structure intensities $R(\mathbf{d^k})$, where R is the rotation matrix which transforms the target Reynolds stress tensor to its principal axes (*i.e.* its diagnolisation), and $\mathbf{d^k} = C_i {\epsilon_i}^k$ with ϵ_i once again a random sign of values

either $+1$ or -1 and $C_i = \sqrt{\left(\sum_{j=1}^{3} \alpha_j\right) - 2\alpha_i}$, with α_i the eigenvalues of the target Reynolds stress tensor. It can be noted that this last equation imposes restrictions on the Reynolds stress tensors which can be used with this method, for the value under the square root to remain positive.

Lastly, in order to perform analyses on both formulations, the filling ratio R_f is defined as the following:

$$Rf = \frac{\frac{4}{3}\pi\lambda^3 N}{V_0}. \tag{9}$$

This ratio represents the density of the *turbulent structures* within the study volume V_0. Values of Rf higher than 1 signify that several *turbulent structures* are overlapping each other.

3. Convergence and analysis of both formulations

A convergence analysis of the computed Turbulent Kinetic Energy (TKE) is now presented depending on several numerical parameters, such as the size of the turbulent structures as well as the number of turbulent structures per volume unit, characterised by the filling ratio R_f. Two different Reynolds stress tensors $\overline{\overline{R}}$ were used in the present study, both chosen to be diagonal as a first simple case study. Ambient turbulence intensity levels I_∞ are defined as the percentage:

$$I_\infty = \frac{100}{|\overline{\mathbf{u}_\infty}|}\sqrt{\frac{\mathrm{tr}\left(\overline{\overline{R}}\right)}{3}}, \tag{10}$$

with $\overline{\mathbf{u}_\infty}$ the average velocity chosen for the upstream current. Among the physical parameters chosen for the following numerical simulations using Jarrin's SEM and Poletto's DFSEM, the only difference lies in the anisotropic ratio, defined as the ratio between the diagonal terms of $\overline{\overline{R}}$. The anisotropic ratio measured *in situ* and given in the paper of Milne *et al.* [13] was initially chosen as a test case for Jarrin's formulation: $(1, 0.75, 0.56)$. Unfortunately, due to the constraints on the eigenvalues of the Reynolds stress tensor mentioned at the end of previous Section 2, the Milne *et al.* Reynolds stress tensor could not be used as such with Poletto's formulation. This is a first limitation, that could be considered as a drawback, for Poletto's more recent formulation. Thus a simpler anisotropic ratio was used for the computations using the DFSEM: $(1, 1, 1)$.

Based on the time series of the velocity computed at a single point for 6 to 12 hours of simulated time, the evolution of the current Turbulent Kinetic Energy (TKE) is verified, as well as its convergence towards the target value given by the user-prescribed Reynolds stress tensor. Such time series shown in Figure 2 show the disparity of the quality and speed of this convergence depending on the parameters R_f and λ which are being used. While all sets of parameters for both methods do show an eventual satisfying convergence towards the direction of the target value represented in black, this convergence does appear to be slower when using the SEM compared to the DFSEM (recalling that 12 hours of simulated time are shown on the left against 6 on the right), and for both methods the convergence is slower as well when using a small number of large sized turbulent structures compared to a high number of smaller structures.

In order to confirm the tendencies previously noted on the time series of the TKE, and given the random aspect of each individual simulation using both the SEM and DFSEM, 50 time series such as those presented in Figure 2 are performed for each set of parameters λ ranging from 0.25 to 1 as well as R_f ranging from 0.1 to 10. The maximal (dotted lines) and average (full lines) of the errors committed on the 50 final values of the TKE for each set of parameters are presented in Figure 3. The trends mentioned previously can thus be confirmed. For both

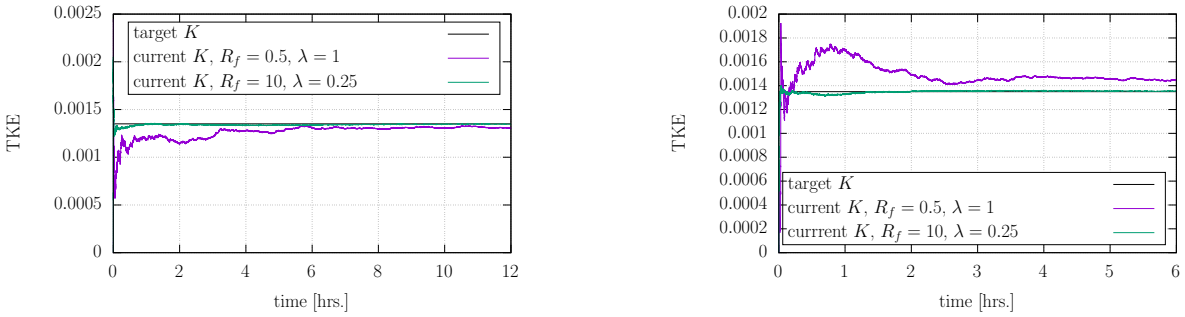

(a) SEM Jarrin (b) DFSEM Poletto

Figure 2. Example of the time series of the Turbulent Kinetic Energy in the "best" and "worst" convergence scenarios.

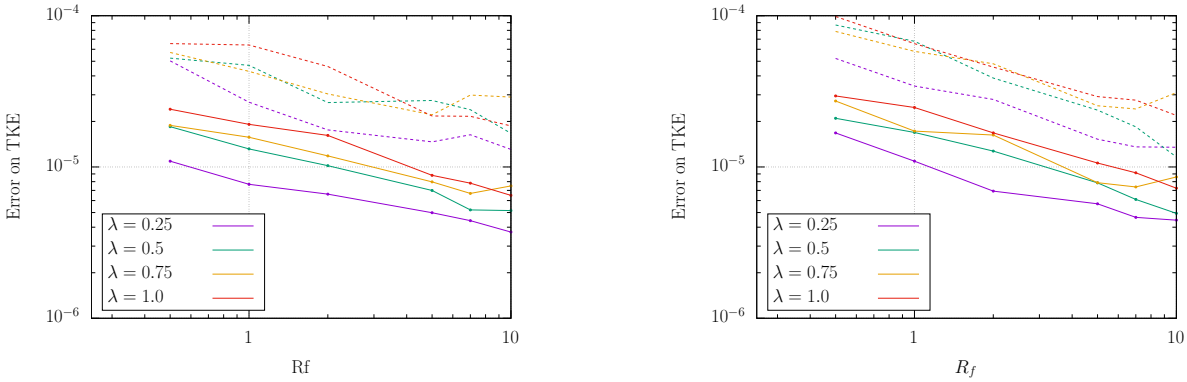

(a) SEM Jarrin: after 12 hours of simulated time.

(b) DFSEM Poletto: after 6 hours of simulated time.

Figure 3. Maximal (dotted lines) and average (full lines) errors committed on the Turbulent Kinetic Energy depending on the size of the turbulent structures used (averaged using 50 sample times series for each set of parameters).

the maximum and averaged values, there is a slight evidence that the higher the filling ratio Rf and the smaller the length scale λ, the lower the error on the final TKE. A regular linear trend (in logarithmic scale) is clearly observed for both the SEM and DFSEM in Figure 3.

The reconstructed velocity fields can now be further analysed by looking for instance at the Power Spectral Density (PSD) spectra (Figure 4). Similarly to the procedure used during experimental trials, time series of the numerically produced velocities are recorded now for a duration of one hour of simulated time, and post-processed in order obtain the PSD spectra. As already observed in Pinon *et al.* [14] and further analysed in Choma Bex *et al.* [2] for Jarrin's initial SEM formulation, the choice of a single value for the structure size λ leads to a poor reproduction of the desired Power Spectral Density. The same behaviour is now evidenced for the DFSEM version of Poletto. However the quality of these PSDs can be largely improved by the introduction of a statistical variation $\sigma(\lambda)$ on the size λ of the turbulent structures. The size of all turbulent structures are no longer all identical throughout the study space and simulation, but calculated using a normal distribution law centred around an average value still noted λ of standard deviation $\sigma(\lambda)$. In the present example, introducing a standard deviation $\sigma(\lambda) = 100\%$

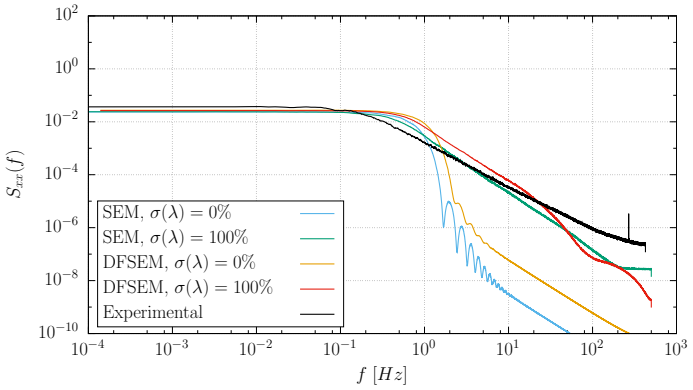

Figure 4. Power Spectral Density (PSD) spectra, $I_\infty = 15\%$, $U_\infty = 0.8$ m/s, $\lambda = 0.5$.

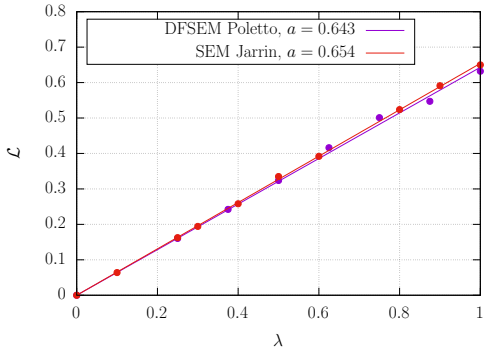

Figure 5. Taylor macro-scale versus length scale λ, $I_\infty = 15\%$, $U_\infty = 1.0$ m/s, $\sigma(\lambda) = 0\%$, $R_f = 1$.

around the average value $\lambda = 0.5$ signifies that the size of a turbulent structure k can now range from $\lambda^k = 0$ to $\lambda^k = 1$. Even though the PSD spectra are much improved with the introduction of heterogeneous structure sizes, the curves do not perfectly fit the experimentally measured values from Gaurier *et al.* [7] represented in black in Figure 4. To the authors' understanding, this is due to the fact that the *turbulent structures'* sizes are evenly spread around the central value, which does not represent the physical phenomenon. A similar but asymmetrical normal distribution will soon be investigated in order to obtain more of smaller sizes, which is expected to mathematically better reproduce the physical turbulent cascade. Additional improvements are expected with the use of this new spreading function.

A last physical turbulent characteristics is now analysed in the form of the Taylor macro-scale $\mathcal{L}$. The same numerical velocity time series as those used to compute the PSD curves are post-processed in order to evaluate this length scale of the turbulent behaviour in the generated flow. The auto-correlation function is evaluated and using the first zero-crossing together with Taylor's frozen hypothesis, the Taylor macro-scale $\mathcal{L}$ is finally obtained. For both the regular SEM and the recently developed DFSEM, near identical linear behaviours are obtained as depicted in Fig. 5, in relation to the prescribed sizes λ of the turbulent structures used for the numerical computations: $\mathcal{L} \approx 0.65\lambda$ for both Jarrin and Poletto's formulations. Similar linear relations but with different multipliers are observed when using different shape functions for the regular SEM formulation, as reported in Choma Bex *et al.* [2]. A similar analysis with different values of $\sigma(\lambda) \neq 0$ will also be necessary to have a full understanding of all the parameters used in both formulations.

4. Computations of turbine's wake

Finally, computations of turbine wakes with varying ambient turbulence intensities ranging from $I_\infty = 0\%$ to $I_\infty = 7\%$ are presented in Figure 6. An isotropic turbulence is used once again for Poletto's DFSEM method, with a turbulence characteristic length of $\lambda = 0.5$ and no variation ($\sigma(\lambda) = 0\%$). Additionally, as the fluctuating turbulence has by definition a zero average ($\langle u'_\infty \rangle = 0$), this component was removed during the post-processing of the time-averaged velocity maps, to emulate the effect of a much longer time average than the last 50 seconds of 90 seconds simulations used here. Only the blades are considered in these simulations, the nacelle and hub of the turbine being omitted at this stage. These turbine blades are considered as infinitely thin blades represented by normal dipoles where a free slip velocity condition is applied. Further details of this vortex particle formulation are given in Pinon et al. [15, 14]. These computations were run with a mesh discretisation of $dh/R = 0.072$, an inter-particle

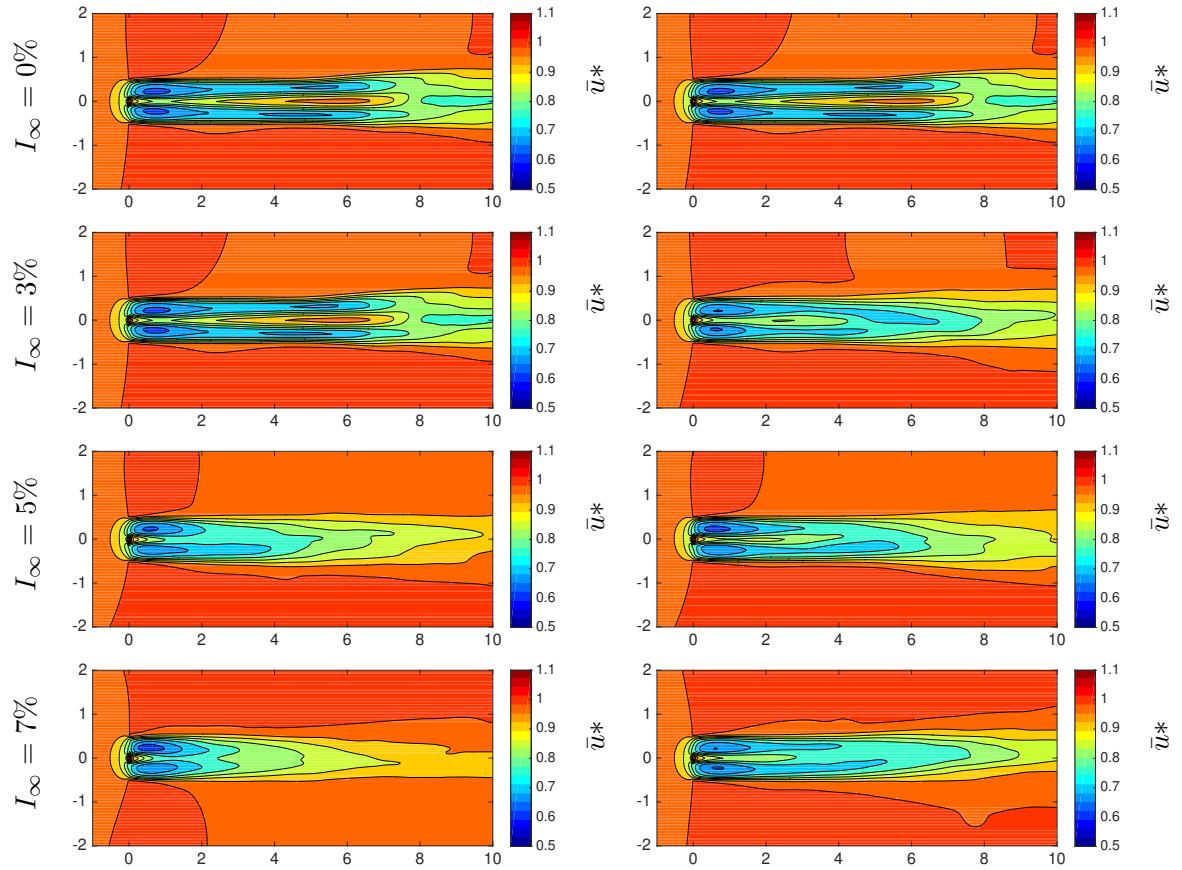

(a) Jarrin (b) Poletto

Figure 6. Time-average of one turbine wake with various ambient turbulence intensities (with no hub and no mast): Poletto's DFSEM turbulence filtered, $TSR = 2.5$, $U_\infty = 1.0$, $R_f = 1$, $\lambda = 0.5$, $\sigma(\lambda) = 0\%$, $(\sigma_u : \sigma_v : \sigma_w) = (1.0 : 1.0 : 1.0)$.

distance of approximately dh and a smoothing parameter for the particle-particle interactions of $1.5\,dh$. A tree-code algorithm combined with an efficient parallelisation procedure using the MPI library is also used, based on a K-means domain decomposition [4]. These computations are run in approximately 15 hours on 252 cores of the regional calculator CRIANN.

As the rotor hub and nacelle are not taken into account, a localised velocity increase can be observed downstream from the center of the turbine. But from the velocity maps presented in Figure 6, it can be confirmed that the increasing ambient turbulence intensity levels have a diffusive and dissipative effect on the wake. For both formulations, the higher the upstream ambient turbulence I_∞, the shorter the turbine wake. However some differences do exist between the effects of the SEM and DFSEM turbulence formulations. At higher ambient turbulence levels, Jarrin's SEM tends to dissipate more than Poletto's DFSEM shown on the right hand side. This tendency is also observable as of $I_\infty \gtrsim 5\%$. In this respect, the results obtained with Poletto's DFSEM could appear more realistic than those of Jarrin's SEM, which remain highly dissipative even at low turbulence intensity levels. However, before a definitive judgement is made on whether Poletto's DFSEM formulation truly improves the quality of the turbine wake behaviour, more computations must be run to ascertain this observation. Among other simplifications, the *turbulent structure* sizes λ are here all fixed at $\lambda = 0.5$ with no variation

$\sigma(\lambda) = 0\%$. Allowing variations in structure sizes $\sigma(\lambda) > 0\%$ or a variation on the central value of λ could lead to slightly different results. Still, from this preliminary investigation, this possibility of taking into account upstream ambient turbulence in the Lagrangian Vortex Blob formalism already is an interesting feature. In that respect, more accurate computations of turbine wake interactions with a downstream turbine, such as the one presented in Fig. 7, will now be possible depending on different ambient turbulence levels.

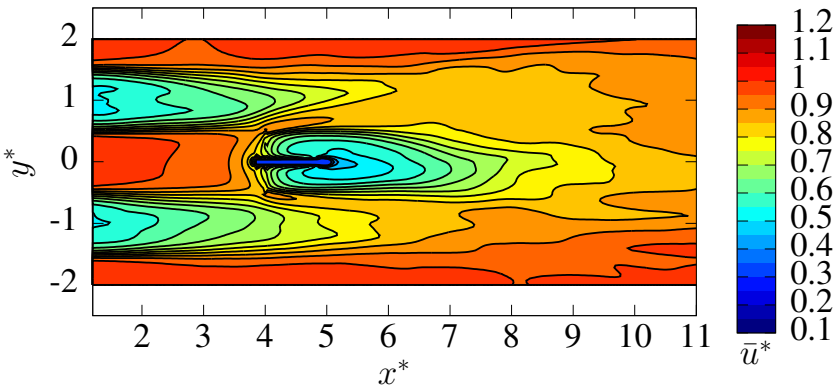

Figure 7. Average velocity field of three interacting turbines with an ambient turbulence intensity of $I_\infty = 3\%$ reproduced from Carlier [4]. Jarrin's SEM formulation was used for this present computation as a proof of concept for further computations of turbine interactions.

5. Conclusions

This study deals with the numerical computations, under the Lagrangian Vortex blob formalism, of turbine wakes and wake interactions with an account for ambient turbulence. Jarrin's formulation of the regular SEM was first developed and tested; some details of these developments and the already obtained results can be found in Choma Bex *et al.* [2]. Unfortunately, the major drawback of this initial version of Synthetic Eddy Method is that it is based on velocity sources and sinks that prevent the ensuing velocity fields from being divergence free. This feature is quite important as the Lagrangian Vortex blob formalism relies on a divergence free velocity field for the Biot-Savart equation. In practice, this initial formulation of Jarrin *et al.* did not show any major incompatibility when implemented in the code, at least for reasonable values of turbulence intensity.

In order to be fully consistent with the Lagrangian Vortex blob hypothesis, a more recent formulation of the Divergence Free Synthetic Eddy Method was implemented in the code. The improvements made when using Poletto *et al.* [16]'s formulation are highlighted by comparison with Jarrin *et al.* [9]'s initial version. At first sight, both formulations seem to behave similarly in terms of reconstructed Power Spectral Densities (PSD) and Taylor macro-scales from velocity records. But the more recent version of Poletto presently shows an improvement in terms of temporal convergence. Finally, numerical computations of turbine wakes with different levels of ambient turbulence are presented, which tend to indicate that the Poletto's formulation of DFSEM seems to be less diffusive than Jarrin's regular SEM formulation. Even if more studies with several parameters variations are still needed to have a better understanding of this model, Poletto's DFSEM already shows some very interesting features for modelling ambient turbulence in a Lagrangian Vortex framework.

6. Acknowledgements

The first author acknowledges the financial support of IFREMER for the financing her Ph.D. grant. The authors acknowledge the support of the CPER-ERDF programs NEPTUNE and SEMARIN funded by the Normandy Regional Council and the European Union. The present work was performed on computing resources provided by CRIANN (Normandy, France).

References

[1] P. Bernard, A. Vir, V. Moureau, G. Lartigue, L. Beaudet, P. Deglaire, and L. Bricteux. Large-eddy simulation of wind turbines wakes including geometrical effects. *Computers And Fluids*, 173:133–139, 2018.

[2] Camille Choma Bex, Clément Carlier, Arnaud Fur, Grégory Pinon, Grégory Germain, and Elie Rivoalen. A stochastic method to account for the ambient turbulence in Lagrangian Vortex computations. *Accepted to Applied Mathematical Modeling - https://doi.org/10.1016/j.apm.2020.05.025*, 2020.

[3] E. Branlard, P. Mercier, E. Machefaux, M. Gaunaa, and S. Voutsinas. Impact of a wind turbine on turbulence: Un-freezing turbulence by means of a simple vortex particle approach. *Journal of Wind Engineering and Industrial Aerodynamics*, 151:37 – 47, 2016.

[4] C. Carlier. *Simulation du comportement d'hydroliennes : modélisation de l'influence de la turbulence ambiante et des effets d'interactions*. PhD thesis, Normandie Université, 2017.

[5] Philippe Chatelain, Stéphane Backaert, Grégoire Winckelmans, and Stefan Kern. Large eddy simulation of wind turbine wakes. *Flow Turbulence and Combustion*, 91:587–605, 2013.

[6] Philippe Chatelain, Matthieu Duponcheel, Stphanie Zeoli, Simon Buffin, Denis-Gabriel Caprace, Grgoire Winckelmans, and Laurent Bricteux. Investigation of the effect of inflow turbulence on vertical axis wind turbine wakes. *Journal of Physics: Conference Series (Print)*, 854(1):012011, 2017.

[7] Benoît Gaurier, Clément Carlier, Grégory Germain, Grégory Pinon, and Elie Rivoalen. Three tidal turbines in interaction: An experimental study of turbulence intensity effects on wakes and turbine performance. *Renewable Energy*, 148:1150 – 1164, 2020.

[8] M.O.L. Hansen, J.N. Srensen, S. Voutsinas, N. Srensen, and H.Aa. Madsen. State of the art in wind turbine aerodynamics and aeroelasticity. *Progress in Aerospace Sciences*, 42(4):285 – 330, 2006.

[9] N. Jarrin, S. Benhamadouche, D. Laurence, and R. Prosser. A synthetic-eddy-method for generating inflow conditions for large-eddy simulations. *International Journal of Heat and Fluid Flow*, 27:585–593, 2006.

[10] Nicolas Jarrin. *Synthetic Inflow boundary conditions for the numerical simulation of turbulence*. PhD thesis, University of Manchester, 2008.

[11] A. Leonard. Vortex methods for flow simulation. *Journal of Computational Physics*, 37(3):289–335, 1980.

[12] Thomas S. Lund, Xiaohua Wu, and Kyle D. Squires. Generation of turbulent inflow data for spatially-developing boundary layer simulations. *Journal of Computational Physics*, 140:233–258, 1998.

[13] I. A. Milne, R. N. Sharma, R. G. J. Flay, and S. Bickerton. Characteristics of the turbulence in the flow at a tidal stream power site. *Philosophical Transactions of the Royal Society A: Mathematical, Physical and Engineering Sciences*, 371(1985):pp, February 2013.

[14] Grégory Pinon, Clément Carlier, Arnaud Fur, Benoît Gaurier, Grégory Germain, and Élie Rivoalen. Account of ambient turbulence for turbine wakes using a synthetic-eddy-method. *Journal of Physics: Conference Series*, 854(1):012016, 2017.

[15] Grégory Pinon, Paul Mycek, Grégory Germain, and Elie Rivoalen. Numerical simulation of the wake of marine current turbines with a particle method. *Renewable Energy*, 46(0):111 – 126, 2012.

[16] Ruggero Poletto. *Divergence free develoment of the Synthetic Eddy Method in order to improve synthetic turbulence for embedded LES simulations*. PhD thesis, 2014.

[17] L. Shi, V. A. Riziotis, S. G. Voustinas, and J. Wang. A consistent vortex model for the aerodynamic analysis of vertical axis wind turbines. *Journal of Wind Engineering and Industrial Aerodynamics*, 135:57–69, 2014.

[18] S.G. Voutsinas. Vortex methods in aeronautics: how to make things work. *International Journal of Computational Fluid Dynamics*, 20(1):3–18, 2006.